Research Article Vol. 28, No. 5 / 2 March 2020 / Optics Express 7539
Optics EXPRESS

Multimodal plasmonic optical fiber grating aptasensor

MAXIME LOBRY,[1] MÉDÉRIC LOYEZ,[2] EMAN M. HASSAN,[3] KARIMA CHAH,[1] MARIA C. DEROSA,[3] ERIK GOORMAGHTIGH,[4] RUDDY WATTIEZ,[2] AND CHRISTOPHE CAUCHETEUR[1,*]

[1]*Electromagnetism and Telecommunication Department, University of Mons, 31 Bld Dolez, 7000 Mons, Belgium*
[2]*Proteomics and Microbiology Department, University of Mons, 6 Av. du Champ de Mars, 7000 Mons, Belgium*
[3]*Institute of Biochemistry, Carleton University, 1125 Colonel By Drive, Ottawa, Ontario K1S 5B6, Canada*
[4]*Laboratory for the Structure and Function of Biological Membranes, Center for Structural Biology and Bioinformatics, Université Libre de Bruxelles, Av. Franklin Roosevelt 50,1050 Brussels, Belgium*
[*]*christophe.caucheteur@umons.ac.be*

Abstract: Tilted fiber Bragg gratings (TFBGs) are now a well-established technology in the scientific literature, bringing numerous advantages, especially for biodetection. Significant sensitivity improvements are achieved by exciting plasmon waves on their metal-coated surface. Nowadays, a large part of advances in this topic relies on new strategies aimed at providing sensitivity enhancements. In this work, TFBGs are produced in both single-mode and multimode telecommunication-grade optical fibers, and their relative performances are evaluated for refractometry and biosensing purposes. TFBGs are biofunctionalized with aptamers oriented against HER2 (Human Epidermal Growth Factor Receptor-2), a relevant protein biomarker for breast cancer diagnosis. *In vitro* assays confirm that the sensing performances of TFBGs in multimode fiber are higher or identical to those of their counterparts in single-mode fiber, respectively, when bulk refractometry or surface biosensing is considered. These observations are confirmed by numerical simulations. TFBGs in multimode fiber bring valuable practical assets, featuring a reduced spectral bandwidth for improved multiplexing possibilities enabling the detection of several biomarkers.

1. Introduction

Optical fiber sensors are involved in numerous sensing applications for which continuous monitoring is required [1–3]. Possibilities in sensor designs are manifold: strain, temperature, pressure, chemical, and bio-chemical sensors can be achieved, among other applications [4–11]. The latter two are usually derived from the use of an optical fiber as a refractometer [12–14]. Refractive index (RI) sensing can provide intrinsic information about the probed medium such as its density, the concentration in chemical compounds or the purity of a solution. Subsequently, RI measurement is widely used in the frame of chemical solutions and products quality control in industries involving food transformation or chemicals processes [15–19].

Among existing technologies, the use of optical fibers for surrounding refractive index (SRI) measurements present several advantages. First, their size allows the production of very small-scaled optrodes with a diameter of 125 µm only. In this way, the sample volume is limited and can be remotely probed. Secondly, there are flexible and cost-effective while telecommunication-grade fiber-based features provide affordable sensing tool in any type of configurations [20]. Finally, the use of optical fibers leads to a very rapid detection, useful for real-time and continuous monitoring [21]. Several sensors can be integrated in the same fiber allowing quasi-distributed measurements [22].

#385747 https://doi.org/10.1364/OE.385747
Journal © 2020 Received 16 Dec 2019; revised 13 Feb 2020; accepted 16 Feb 2020; published 27 Feb 2020

Optics EXPRESS

Typically, in a standard telecommunication optical fiber, light is guided and remains confined inside the fiber core. Therefore, to couple light towards the surrounding medium, the fiber structure is modified. Geometries leading to optical fiber refractometers are various such as etched, tapered, D-shaped or U-shaped optical fibers [21]. Also, fiber grating refractometers can be manufactured within the fiber core using side laser radiation [23–25]. Our work makes use of tilted fiber Bragg gratings (TFBGs).

A TFBG is a periodic and permanent modulation of the refractive index directly induced in the fiber core [26]. It usually exhibits a slight angle with respect to the perpendicular to the fiber axis and is conventionally inscribed with UV laser radiation and a tilted phase mask. A TFBG outcouples a part of the core-guided light into the fiber cladding, which therefore interacts with the surrounding medium. In addition to the Bragg mode that appears at its right end, the transmitted amplitude spectrum of a TFBG is composed of numerous tens of narrow-band cladding mode resonances resulting in a comb-like spectrum [4,21,26]. Each mode has a given effective refractive index, according to the TFBG phase matching conditions, and presents its own sensitivity to SRI [27,28]. The Bragg mode corresponds to the backward coupling of the core mode and is therefore only affected by temperature and strain effects. This feature makes TFBG a self-referenced system in strain and temperature for refractive index measurements. Sensitivity to SRI can be significantly improved through the excitation of surface plasmon resonance (SPR) [12,19,21,29]. An SPR is an oscillation of electrons at a metal-dielectric interface. It can be excited by covering the fiber with a thin metal layer, most often gold. To excite a plasmon, incident light to the metal-dielectric interface must be radially-polarized (P-polarization) and feature an identical tangential component to that of the plasmon wave [12]. This excitation is characterized by a strong light absorption for some wavelengths as a function of the SRI, which results in a spectral feature in the TFBG spectrum that is strongly sensitive to surface refractive index changes.

So far, gold-coated TFBGs have been functionalized with various biorecognition elements including antibodies and aptamers to turn them into immunosensors and aptasensors, respectively for proteins or cells sensing [19,30–35]. Highly sensitive detections have been reported for both *in vitro* and *ex vivo* assays [19]. In this article, we demonstrate for the first time the accurate detection of HER2 (Human Epidermal Growth Factor Receptor-2, also known as ErbB2), a protein biomarker targeted for breast cancer diagnosis. This is obtained with specific aptamers grafted on the gold surface. While all experiments with gold-coated TFBGs reported until now have been made with single-mode optical fibers, we also use in our work multimode optical fiber (MMF). Hence, we can compare the relative performances of these two fiber types, for both bulk refractometry and surface biosensing. While MMF-TFBGs outperform by ~22% the refractometric sensitivity of their SMF counterparts, they present similar performances for the detection of HER2 at growing concentrations in buffer solutions starting from 10^{-12} g/ml. Through numerical simulations conducted with a complex finite-difference mode solver, we demonstrate that these observations can be explained by the power fraction of the optical mode in the considered surrounding medium. Compared to SMF-based sensors, MMF-TFBGs offer interesting practical benefits provided that splices with SMF pigtails are properly made. They present a more limited spectral bandwidth allowing wavelength multiplexing while being more adequate with an etching process that further improves the sensing performances thanks to a higher core-cladding diameter ratio [36].

2. Experimental refractometric measurements

Experiments were conducted on bare and gold-coated TFBGs photo-inscribed in both types of fibers. Besides demonstrating the possibility of grating inscription and surface plasmon resonance excitation in MMF, the objective of these tests was to compare the refractometric sensitivities of TFBG-assisted sensors, photo-inscribed in both SMF and MMF.

Optics EXPRESS

Both single mode (Corning SMF-28) and multimode (Corning MMF 50/125) fibers are silica telecommunication-grade fibers. The SMF has a core diameter of 8.2 µm for a total cladding diameter of 125 µm without the polymer jacket. In contrast, the MMF features dimensions of 50 µm and 125 µm as core and cladding diameter, respectively. Before the grating manufacturing and in order to increase their photosensitivity, optical fibers were both hydrogen-loaded under ~200 bar and 60 °C for 30 hours. TFBGs were inscribed in the core of stripped fiber regions with the NORIA system from Northlab Photonics featuring an excimer laser emitting at 193 nm and a uniform phase-mask of 1088 nm period that was tilted in the plane perpendicular to the UV laser beam. 1 cm long 7° TFBG were produced to generate cladding modes with effective refractive index close to the one of water solutions.

Refractometric sensitivities of bare TFBGs were assessed by immersing them into LiCl solutions of different concentrations around the RI value of 1.343. This salt is chosen for its high solubility allowing easy preparation of very close RI solutions [37]. Sensor responses were recorded using an FBG interrogator (Micron Optics, 10 Hz sampling rate, 5 pm wavelength resolution) for both bare SMF (b-SMF) and MMF (b-MMF) TFBGs immersed in solutions of different SRI values (Figs. 1(a) and 1(c)). We can notice that the spectrum of a grating inscribed in MMF exhibits a narrower comb of resonances (30–40 nm) than a grating created in SMF (90–100 nm). As shown in Fig. 1(c), cladding mode coupling is not effective for the MMF between ~1560 nm and the Bragg wavelength located at ~1588 nm. This results from the weaker thickness of the cladding. As a consequence, MMF is more adequate to produce wavelength-multiplexed sensors while keeping the ability to measure in aqueous solutions. In practice, for standard FBG interrogators in the C + L wavelength bands, two TFBGs in MMF could be wavelength multiplexed and interrogated simultaneously while only one can be used when dealing with SMF and solutions with a RI close to the one of water. In case of bare TFBG

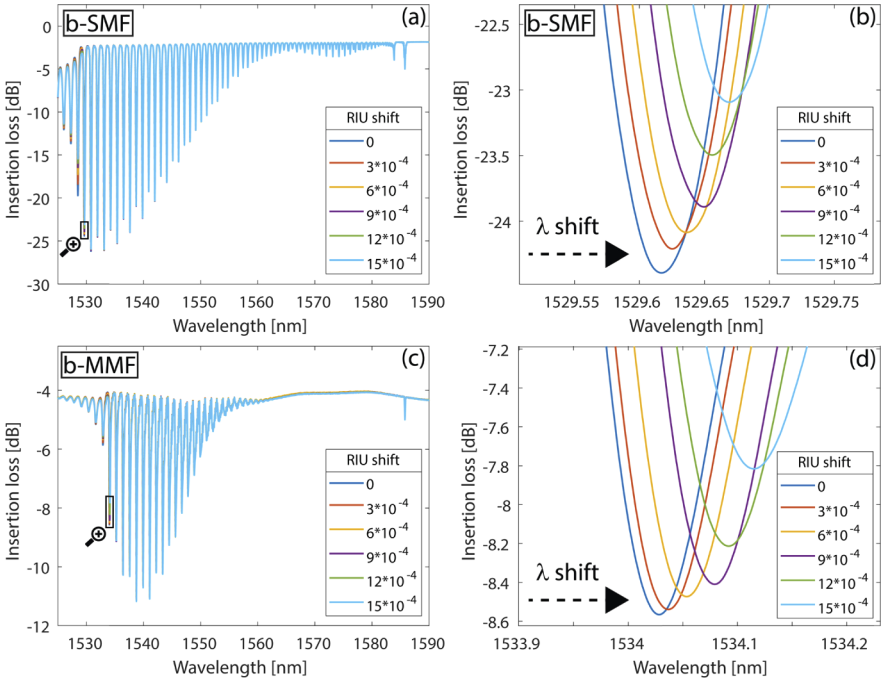

Fig. 1. Transmitted spectra of a bare SMF TFBG sensor (b-SMF) (a) with a zoom around the the cutoff mode (b) during the refractometry test. Transmitted spectra of a bare MMF TFBG sensor (b-MMF) (c) with a zoom around the cutoff mode (d) during the same test.

Optics EXPRESS

sensor, assessment of sensitivity value is achieved by tracking the cut-off mode, as done in [38] (Figs. 1(b) and 1(d)). The latter is the most sensitive mode for a considered SRI range, as its effective refractive index is close to the one of the SRI value.

Sensitivity measurements were performed in a 15.10^{-4} RIU range with 3.10^{-4} RIU shifts under the same conditions for both sensor types (Figs. 2(a) and 2(b)). Bare SMF-TFBGs exhibit a mean sensitivity of 33.73 nm/RIU while bare MMF-TFBGs show a value of 56.30 nm/RIU. An improvement of 67% in the refractometric sensitivity is therefore observed in MMF. Linear fits demonstrate the good reproducibility and reliability of bare TFBG sensors with R^2 values of 0.999 and 0.993 for b-SMF and b-MMF, respectively.

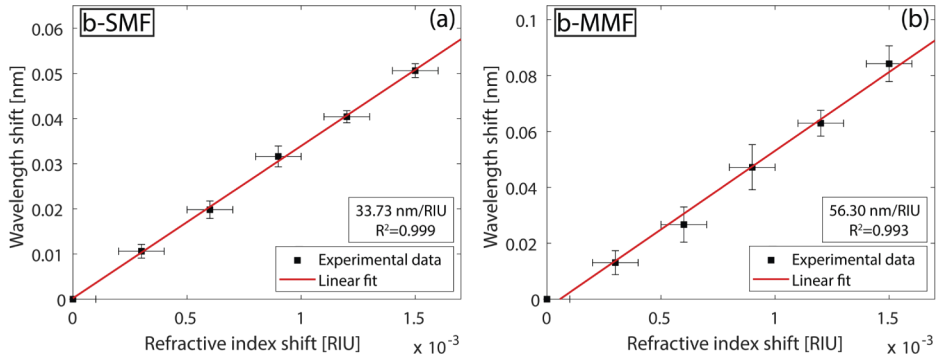

Fig. 2. Cutoff mode wavelength shift (in nm) as a function of RI shift for sensors based on bare TFBG in SMF (b-SMF) (a) and MMF (b-MMF) (b) immersed in increasing RI solutions.

The fiber at TFBG location was also covered with a thin metal layer for SPR excitation. As plasmonic sensors are extensively used for biochemical detection purposes, an Au-layer is commonly used as metal sheath for stainless and biocompatibility reasons. Gold deposition of ~35 nm thick layer was made through a sputtering process (Leica EM SCD 500). The thickness was estimated by a Quartz microbalance installed in the chamber of the sputter coater. The homogeneity of the deposited layer can be appreciated by a scanning electron microscopy (SEM) analysis achieved on a gold-sputtered TFBG (Fig. 3(a)). The metal thickness can be estimated as well (Fig. 3(b)). As observed in our previous works [5,12], this thickness is a good trade-off to ensure a clean SPR signature with a good sensitivity. The sensitivities reported hereafter are only strictly valid for this particular thickness. Gold was deposited on fibers placed horizontally in the

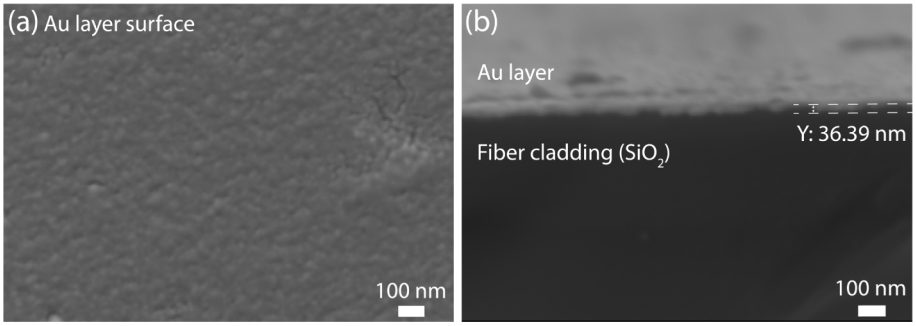

Fig. 3. SEM pictures of the surface (a) and the cross section (b) of a gold sputter-coated TFBG.

Optics EXPRESS

machine. A double deposition with a fiber rotation of 180° was made to ensure a rather uniform gold thickness all around the optical fiber cross-section.

The presence of a finely-tuned gold layer at the fiber grating surface results in an amplitude spectrum exhibiting an SPR attenuation. The latter can be visualized on transmitted amplitude spectra for both gold-coated TFBGs in SMF (Au-SMF) and MMF (Au-MMF) (Figs. 4(a) and 4(c)).

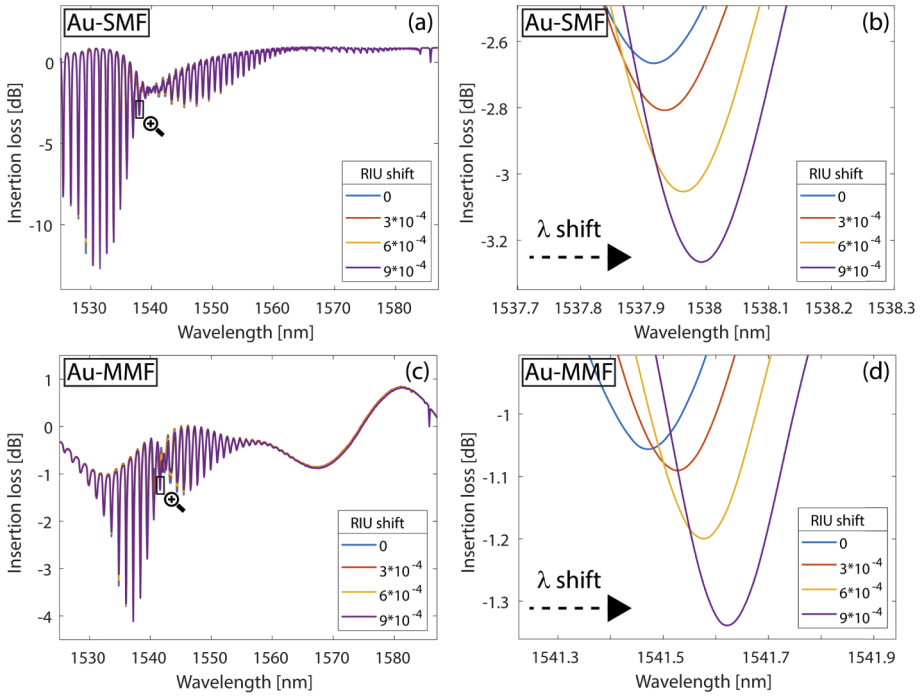

Fig. 4. Transmitted spectra of a gold-coated SMF TFBG sensor (a) and zoom around the most sensitive mode during the refractometry test (b). Transmitted spectra of a gold-coated MMF TFBG sensor (c) and zoom around the most sensitive mode as for the SMF (d).

To demodulate gold-coated TFBGs refractometers, we rely on the classical approach, already reported in [38] and the vast majority of papers involving TFBG refractometers and biosensors. Indeed, the most sensitive mode of the SPR signature cannot be tracked accurately, due to its strong attenuation in the amplitude spectrum and noisy nature. The tracking is therefore based on another cladding mode resonance, located on the shoulder of the SPR envelope (Figs. 4(b) and 4(d)) [38]. This mode is typically located between the SPR signature (characterized by a pinch in the spectrum) and the cut-off mode (the mode to the left of the SPR signature with the largest peak-to-peak amplitude, whose effective refractive index value is slightly above the one of the surrounding medium) [39].

A sensitivity value of 102.03 nm/RIU ($R^2 = 0.999$) was obtained for the gold-coated SMF-TFBG sensor (Figs. 5(a) and 5(b)). A higher value was attained for the MMF-based sensor with a sensitivity of 124.89 nm/RIU ($R^2 = 0.998$) under the same conditions. We therefore observe a refractometric sensitivity enhancement of about 22% by using a multimode fiber as a substrate for gold-coated grating manufacture.

The so-called figure of merit (FOM) corresponding to the ratio between the sensitivity and the full width at half maximum (FWHM) was computed for each configuration. Bare SMF and MMF TFBG sensors exhibit respectively relative different FOM values of 167 and 261. In contrast, gold-coated TFBGs show FOMs of 510 and 541 in SMF and MMF, respectively.

Optics EXPRESS

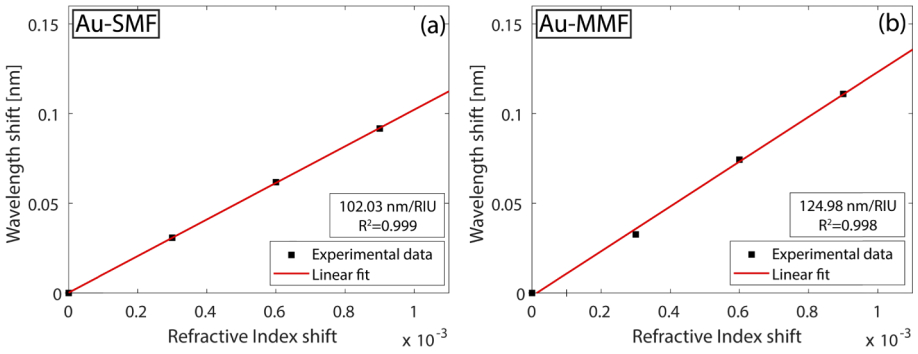

Fig. 5. Most sensitive mode wavelength shift (in nm) as a function of RI shift for sensors based on gold-coated TFBG inscribed in SMF (a) and MMF (b) immersed in increasing RI solutions.

3. Numerical simulations

Our experimental observations were then compared to numerical simulations obtained with a mode solver. To this aim, the FimmWave finite-difference complex mode solver (from Photon Design Inc.) was used to model the optical fiber geometries tested in section 2. Taking into account parameters for both SMF and MMF and refractive properties of materials and media used for the experimental part, we simulated conditions as close as possible to the experiments. Relying on the specifications of the used optical fibers, standard single mode fiber was simulated

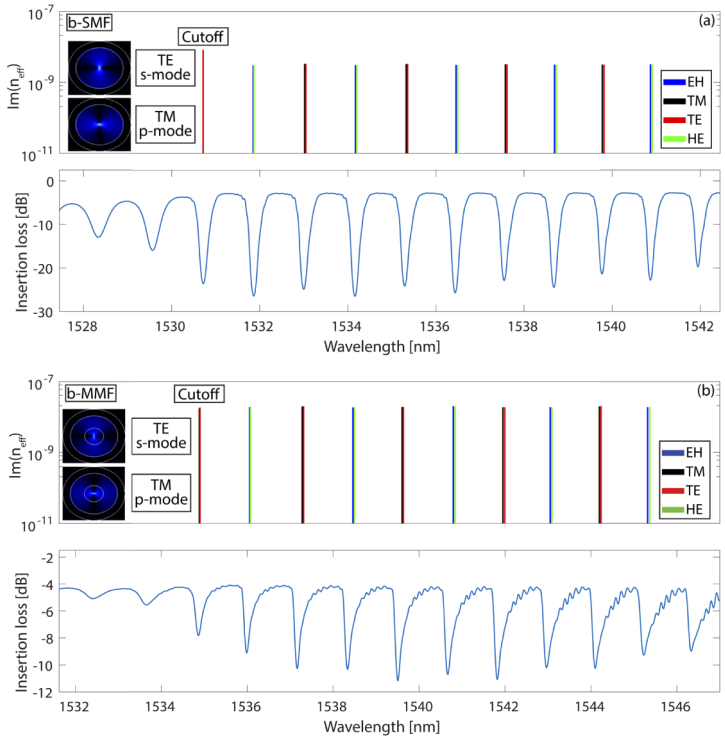

Fig. 6. Simulated (bar mode spectrum) and experimental (blue curve) spectra of a bare SMF-TFBG sensor (b-SMF) (a) and a bare MMF-TFBG sensor (b-MMF) (b).

Optics EXPRESS

with a germanium doped silica core characterized by a 1.449 RI value and a silica cladding with a 0.36% lower RI. Multimode optical fiber was considered with a core RI equal to 1.458, the latter being 1% higher than the cladding RI value.

The solver computes the complex refractive index of the light modes supported by the considered optical fiber geometry. The real part of this complex refractive index is the effective refractive index of the mode while its imaginary part is the extinction coefficient, which is an image of the mode attenuation. More specifically, two families of modes are computed: TM_{0n} and EH_{1n} modes that are radially-polarized and TE_{0n} and HE_{1n} modes that are azimuthally-polarized. These two families are respectively labeled P- and S-modes in the following. As depicted in Fig. 6, our aim is to make a one-to-one comparison between the modes present in the transmitted amplitude spectrum and the simulated ones for the P-Polarization family. To this aim, the real part of the complex refractive index, which is linked to the wavelengths of the cladding modes is used to generate the x axis of the plot while the y axis corresponds to the imaginary part. Hence, the real part of the computed index was introduced in the TFBG phase matching conditions ($\lambda_{clad,i} = (n_{eff,core} + n_{eff,clad,i})\Lambda/\cos\theta$) where $n_{eff,core}$ is the core effective refractive index, $\lambda_{clad,i}$ represents the resonance corresponding to $n_{eff,clad,i}$, Λ is the grating period and θ is the tilt angle. Figures 6(a) and 6(b) show a very good correspondence between simulated and experimental modes, confirming the robustness of the mode solver.

In order to design plasmonic sensors, a thin gold layer (~35 nm) was then added between the optical fiber and the surrounding medium. Gold is characterized by a complex refractive index of 0.56-11.4j. Figures 7(a) and 7(b) confirm that the SPR excitation can be visualized through simulations. The most affected modes by the plasmonic effect are highly attenuated due

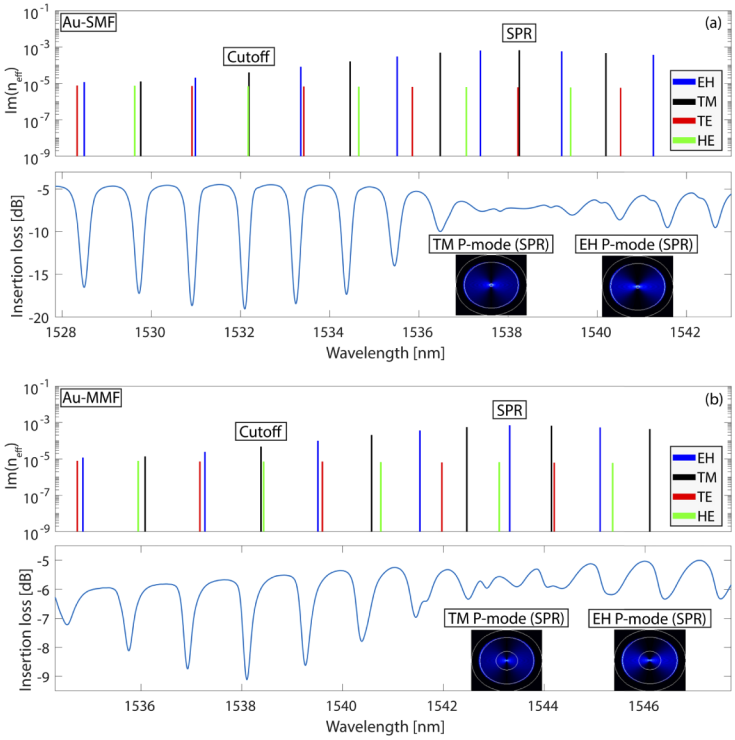

Fig. 7. Simulated (bar mode spectrum) and experimental (blue curve) spectra of a gold-coated SMF TFBG sensor (Au-SMF) (a) and a gold-coated MMF TFBG sensor (Au-MMF) (b).

Optics EXPRESS

to the energy absorption so that these modes are characterized by a high extinction coefficient in the numerical values. The impact of this phenomenon decreases on both sides of the most attenuated mode, which explains the shape of simulated spectra in terms of the RI imaginary part. Moreover, only radially-polarized light allows plasmon excitation so that only P-modes are attenuated. S-modes remain unaffected and unsensitive to SRI change, as they cannot tunnel inside the gold layer.

Theoretical sensitivity values of both mentioned configurations were also computed in the same conditions as those involved in experimental tests. The refractive index of the surrounding medium is therefore slightly changed, and a new simulation is run for every considered SRI value. As depicted in Fig. 8, results indicate sensitivity values close to the experimental ones. Slight discrepancies result from the difficulty to exactly model the real experimental conditions, considering the uncertainties on the actual thickness and overall homogeneity of the gold layer deposition process. MMF-TFBG refractometers are more sensitive than SMF-TFBG ones and the improvement essentially appears for bare configurations. Indeed, using MMF instead of SMF results in a sensitivity increase of 66.91% (experimentally) and 109.50% (simulated) for bare TFBGs. Gold-coated MMF-TFBG refractometers are more sensitive than SMF-TFBG ones with simulated sensitivity values of 141.19 and 116.80 nm/RIU respectively. This yields an enhancement of 20.88% for the MMF-TFBG compared to the SMF-TFBG, in very good agreement with the experimental trend (22.41%). All measured and simulated sensitivity values are reported in Table 1.

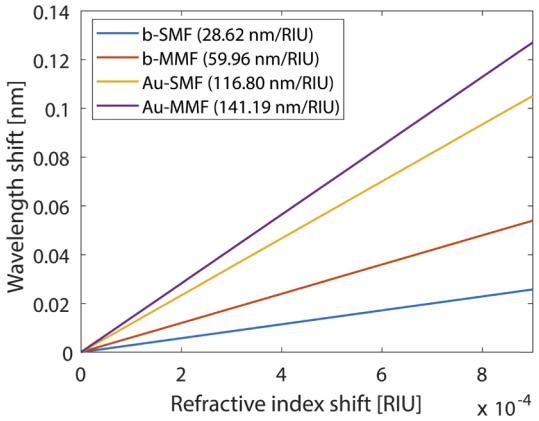

Fig. 8. Simulated refractometric sensitivity for bare and gold-coated sensors in SMF and MMF.

Table 1. Experimental and simulated refractometric sensitivity values of bare and gold-coated TFBGs inscribed in SMF and MMF.

	SMF		MMF	
TFBG	Experimental sensitivity [nm/RIU]	Simulated sensitivity [nm/RIU]	Experimental sensitivity [nm/RIU]	Simulated sensitivity [nm/RIU]
Bare	33.73	28.62	56.30	59.96
Au-coated	102.03	116.80	124.89	141.19

Optics EXPRESS

4. HER2 aptasensors and bioassays

4.1. Aptasensors biofunctionalization

Both fiber types were biofunctionalized with anti-HER2 ssDNA aptamers onto the gold surface with the aim to specifically detect HER2 proteins. These aptamers were selected by the Systematic Evolution of Ligands by EXponential enrichment (SELEX) method as already achieved in previous works [40,41]. Thiolated anti-HER2 aptamers were then synthesized with the help of a MerMade 6 automated DNA synthesizer (BioAutomation USA) through phosphoramidite chemistry leading to the following ssDNA aptamer sequence: 5'-TCT AAA AGG ATT CTT CCC AAG GGG ATC CAA TTC AAA CAG C-S-S-3'. This step was performed using DNA bases and thiol modifiers from Glen Research (Sterling, VA, USA).

Before immobilization, thiol-modified aptamers were resuspended in TE buffer (Tris-ethylenediaminetraacetic) 100 µM from Base Pair Biotechnologies and diluted 1:1 v/v with TCEP (Tris (2-carboxyethyl) phosphine) solution from Base Pair Biotechnologies to be reduced at 90 °C for 5 min. During this step, aptamers are folded into their tertiary structure to allow an optimal binding to HER2 proteins. The working aptamer concentration of 10.24 µM was reached by adding Phosphate Buffer Saline (PBS), pH 7.2 from Thermo Scientific.

Each gold-coated TFBG was then immersed in a small volume (300 µL) of the aptamers solution for the immobilization step during 1h in PBS at room temperature. This step was recorded for both SMF and MMF by tracking wavelength shifts in the TFBG transmitted amplitude spectrum (Figs. 9(a) and 9(b)). Our observations indicate a sudden jump in the wavelength shift when moving from PBS to the solution used for aptamers immobilization. This results from the refractive index difference between both solutions. A progressive wavelength shift is then measured in the aptamers solution, with a total shift of ~20 pm indicating that aptamers are well grafted on the gold surface after several tens of minutes. In order to avoid non-specific recognition, a blocking step using 6-mercapto-1-hexanol 5 mM from Sigma Aldrich was finally performed during 30 min in PBS at room temperature.

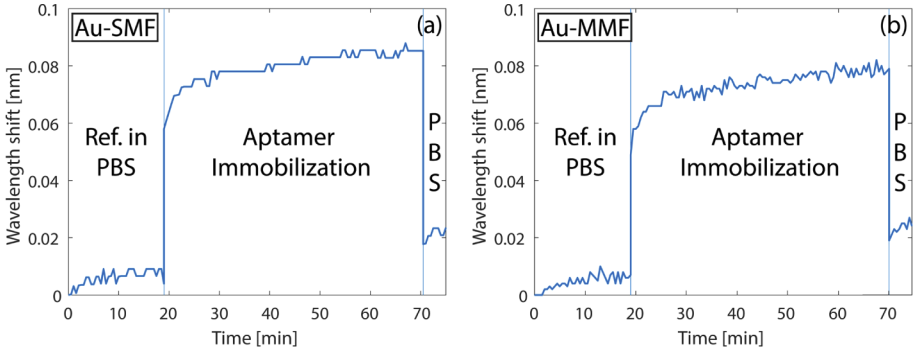

Fig. 9. Aptamer immobilization detection resulting from the tracking of the wavelength shift of the most sensitive mode for a SMF (a) and MMF-based (b) gold-coated TFBG.

For biodetection assays, each biofunctionalized sensor was brought into contact with different HER2 solutions starting from 10^{-12} g/ml in PBS. The used HER2 protein is a full recombinant human protein (116 kDa) purchased from Abcam (ab60866). To confirm the selectivity of our sensors, cytokeratin 17 (CK17) proteins were used. They were purchased from Abcam.

Optics EXPRESS

4.2. HER2 cancer biomarker detection assays

Bioassays were performed with different HER2 protein concentrations ranging from 10^{-12} to 10^{-6} g/mL, PBS is taken as a reference solution. A sketch of the biosensing principle of the elaborated aptasensor is presented in Fig. 10.

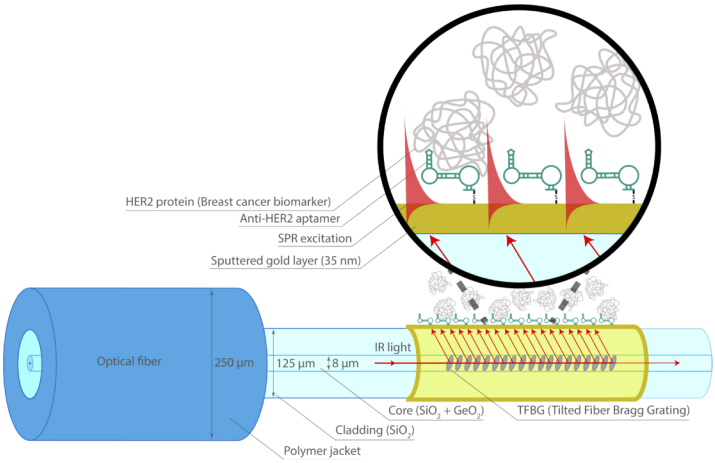

Fig. 10. Sketch of the HER2 protein biodetection using a SPR TFBG-based aptasensor in SMF.

Several solutions were tested on the two optical fiber-based biosensor configurations in order to compare their behavior in terms of biodetection. For a given concentration, an aptasensor was immersed in a protein solution for 10 min at room temperature to reach a stable bio-chemical detection. The sensitivity was assessed by tracking the wavelength shift of the most sensitive mode for each configuration and each concentration. This signal shift reflects the binding of molecules at the biosensor surface. Figure 11 depicts the change observed for a 10^{-6} g/ml concentration of HER2 compared to PBS and to the same concentration of cytokeratins 17 (CK17), a potential lung cancer biomarker already used in our previous works [19,20,38]. These observations confirm that a very good selectivity was achieved, since the response obtained with CK17 is only 5% of the shift recorded with the same concentration of HER2.

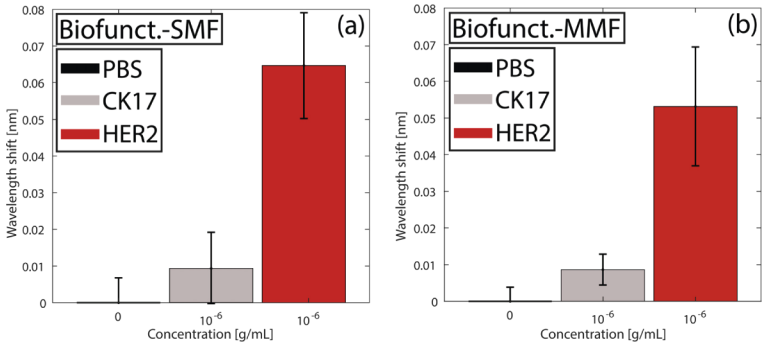

Fig. 11. Spectral response in wavelength shift for SMF (a) and MMF-based (b) aptasensors for an HER2 concentration of 10^{-6} g/ml in PBS after a negative control (CK17). Error bars represent the standard deviation on 3 measurements made in the same conditions.

Figure 12 shows a progressive increase of the wavelength shift response for both sensor types from 10 pm to 70 pm when the HER2 concentration grows from 10^{-12} to 10^{-6} g/mL with the

Optics EXPRESS

ability to detect the lowest tested concentration compared to the average value measured in PBS. A quite similar behavior between both fiber types is also obtained for biosensing while MMF-TFBGs are more sensitive than SMF ones when bulk refractometry is considered.

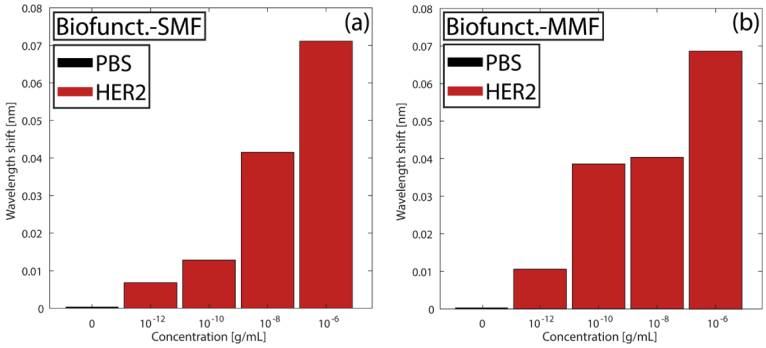

Fig. 12. Spectral response in wavelength shift for SMF (a) and MMF-based (b) aptasensors for growing HER2 concentrations in PBS.

To figure out this experimental behavior, FimmWave was used again, to compute the fill factor (i.e. the power fraction) of the considered modes in the investigated medium. The aptamer layer was modeled as a 1 nm thick medium with a refractive index value of 4 10^{-5} RIU higher than the one of the surrounding medium corresponding to PBS, as computed from the total wavelength shift (20 pm) measured during the aptamers immobilization process. Table 2 contains the computed values considered either in the surrounding medium (PBS) or in the aptamers layer for both fiber types. It can be seen that the power fraction in the surrounding medium is higher for the MMF (58.4%) compared to the SMF (50.2%), which again explains the higher refractometric sensitivity. The corresponding values in the ultra-thin aptamers layer are equivalent for both fiber types, therefore confirming that the surface sensitivity is equivalent in both cases.

Table 2. Power fraction of the SPR mode is the considered surrounding medium

	Gold-coated SMF	Gold-coated MMF
PBS	50.2%	58.4%
Aptamers layer	0.4%	0.4%

5. Conclusion

In this work, we reported photo-inscription of TFBGs in telecommunication-grade MMF as well as the possibility to generate a plasmonic excitation when a gold layer is deposited on the TFBG surface. Then, we compared the refractometric sensitivities of TFBGs inscribed in gold-coated MMF with those of single mode fiber-based sensors. Experiments, confirmed by numerical calculations, demonstrate that MMF-TFBG refractometers outperform the best sensitivities reported for SMF-TFBGs. Gold-coated MMF-TFBGs depict a refractometric sensitivity of 124.89 nm/RIU, an enhancement of ~22% compared to SMF-TFBGs. Gold-coated TFBGs were also biofunctionalized with anti-HER2 aptamers to evaluate their performances for the detection of the relevant breast cancer biomarker HER2. Both fiber types exhibit an equivalent response to increasing concentrations of HER2 proteins from 10^{-12} to 10^{-6} g/mL, with an experimental detection threshold that perfectly fits with the target application. With the same external dimensions allowing them to be embedded in catheters, MMF-TFBGs biosensors bring practical benefits compared to their SMF counterparts. In addition to the gain in refractometric

Optics EXPRESS

sensitivity, MMF-TFBGs display a much narrower spectral comb, which makes them more convenient for multiplexing purpose (and therefore for multiple analytes assays) in a given wavelength span. Also, with their bigger core dimensions, MMF-TFBGs are more suitable to operate in practice after an etching process. The latter can further increase the sensing performances, as recently demonstrated in [36] for bare TFBGs in SMF.

Funding

Fonds De La Recherche Scientifique - FNRS (O001518F).

Acknowledgments

The authors would like to thank the laboratory of Marine Biology (University of Mons, Belgium) for the access to SEM equipment provided by Prof. Igor Eeckhaut and Prof. Patrick Flammang. We also warmly thank Nathan Puozzo for his precious help. The authors are also grateful to Mariel David for her help in preparing optical fiber-based sensors. This work was financially supported by the Fonds de la Recherche Scientifique – FNRS under Grant n° O001518F (EOS-convention 30467715), FRIA Grant of M. Loyez and Grant of the Associate researcher position of C. Caucheteur.

Disclosures

The authors declare that there are no conflicts of interest related to this article.

References

1. B. Lee, "Review of the present status of optical fiber sensors," Opt. Fiber Technol. **9**(2), 57–79 (2003).
2. J. P. Dakin, K. Hotate, R. A. Lieberman, and M. A. Marcus, "Optical fiber sensor," in *Handbook of Optoelectronics*, J. P. Dakin and R. G. W. Brown, eds., 2nd ed. (CRC Press, 2017), pp. 1–84.
3. K. T. V. Grattan and Y. N. Ning, "Optical current sensor technology," in *Optical Fiber Sensor Technology*, K. T. V Grattan and B. T. Meggitt, eds., 1st ed. (Springer, 1998), pp. 183–223.
4. T. Guo, F. Liu, B. O. Guan, and J. Albert, "Tilted fiber grating mechanical and biochemical sensors," Opt. Laser Technol. **78**, 19–33 (2016).
5. C. Ribaut, M. Loyez, J. C. Larrieu, S. Chevineau, P. Lambert, M. Remmelink, R. Wattiez, and C. Caucheteur, "Cancer biomarker sensing using packaged plasmonic optical fiber gratings: towards in vivo diagnosis," Biosens. Bioelectron. **92**, 449–456 (2017).
6. Z. Li, Z. Yu, Y. Shen, X. Ruan, and Y. Dai, "Graphene enhanced leaky mode resonance in tilted fiber Bragg grating: a new opportunity for highly sensitive fiber optic sensor," IEEE Access **7**, 26641–26651 (2019).
7. T. Guo, "Fiber grating-assisted surface plasmon resonance for biochemical and electrochemical sensing," J. Lightwave Technol. **35**(16), 3323–3333 (2017).
8. Z. Li, J. Shen, Q. Ji, X. Ruan, Y. Zhang, Y. Dai, and Z. Cai, "Tuning the resonance of polarization-degenerate LP1,l cladding mode in excessively tilted long period fiber grating for highly sensitive refractive index sensing," J. Opt. Soc. Am. A **35**(3), 397–405 (2018).
9. M. Lobry, D. Lahem, M. Loyez, M. Debliquy, K. Chah, M. David, and C. Caucheteur, "Non-enzymatic D-glucose plasmonic optical fiber grating biosensor," Biosens. Bioelectron. **142**, 111506 (2019).
10. M. Loyez, M. Lobry, R. Wattiez, and C. Caucheteur, "Optical fiber gratings immunoassays," Sensors **19**(11), 2595 (2019).
11. T. Guo, F. Liu, X. Liang, X. Qiu, Y. Huang, C. Xie, P. Xu, W. Mao, B.-O. Guan, and J. Albert, "Highly sensitive detection of urinary protein variations using tilted fiber grating sensors with plasmonic nanocoatings," Biosens. Bioelectron. **78**, 221–228 (2016).
12. C. Caucheteur, V. Voisin, and J. Albert, "Near-infrared grating-assisted SPR optical fiber sensors: design rules for ultimate refractometric sensitivity," Opt. Express **23**(3), 2918 (2015).
13. C. Caucheteur and P. Mégret, "Demodulation technique for weakly tilted fiber Bragg grating refractometer," IEEE Photonics Technol. Lett. **17**(12), 2703–2705 (2005).
14. B. Jiang, X. Lu, X. Gan, M. Qi, Y. Wang, L. Han, D. Mao, W. Zhang, Z. Ren, and J. Zhao, "Graphene-coated tilted fiber-Bragg grating for enhanced sensing in low-refractive-index region," Opt. Lett. **40**(17), 3994–3997 (2015).
15. F. Jiménez-márquez, J. Vázquez, J. Úbeda, and J. L. Sánchez-rojas, "Chemical temperature dependence of grape must refractive index and its application to winemaking monitoring," Sens. Actuators, B **225**, 121–127 (2016).
16. H. J. Shin, S. Choi, and G. Ok, "Qualitative identification of food materials by complex refractive index mapping in the terahertz range," Food Chem. **245**, 282–288 (2018).

Optics EXPRESS

17. C. Tan and Y. Huang, "Dependence of refractive index on concentration and temperature in electrolyte solution, polar solution, nonpolar solution, and protein solution," J. Chem. Eng. Data **60**(10), 2827–2833 (2015).
18. B. Yuan, S. Tong, X. Zhang, L. Li, and C. Wang, "Automatic monitoring refractive index variations of transient solution during electrochemical reactions," Measurement **98**, 10–16 (2017).
19. M. Loyez, J. Larrieu, S. Chevineau, M. Remmelink, D. Leduc, B. Bondue, P. Lambert, J. Devière, R. Wattiez, and C. Caucheteur, "In situ cancer diagnosis through online plasmonics," Biosens. Bioelectron. **131**, 104–112 (2019).
20. M. Loyez, J. Albert, C. Caucheteur, and R. Wattiez, "Cytokeratins biosensing using tilted fiber gratings," Biosens. Bioelectron. **8**(3), 74–79 (2018).
21. C. Caucheteur, T. Guo, and J. Albert, "Review of plasmonic fiber optic biochemical sensors: improving the limit of detection," Anal. Bioanal. Chem. **407**(14), 3883–3897 (2015).
22. B. Spackova and J. Homola, "Theoretical analysis of a fiber optic surface plasmon resonance sensor utilizing a Bragg grating," Opt. Express **17**(25), 23254–23264 (2009).
23. A. Iadicicco, S. Campopiano, A. Cutolo, M. Giordano, and A. Cusano, "Refractive index sensor based on microstructured fiber Bragg grating," IEEE Photonics Technol. Lett. **17**(6), 1250–1252 (2005).
24. V. Bhatia and A. M. Vengsarkar, "Optical fiber long-period grating sensors," Opt. Lett. **21**(9), 692–694 (1996).
25. F. Chiavaioli, C. A. J. Gouveia, P. A. S. Jorge, and F. Baldini, "Towards a uniform metrological assessment of grating-based optical fiber sensors: from refractometers to biosensors," Biosensors **7**(4), 23–29 (2017).
26. T. Erdogan and J. E. Sipe, "Tilted fiber phase gratings," J. Opt. Soc. Am. A **13**(2), 296 (1996).
27. C. Chan, C. Chen, A. Jafari, A. Laronche, D. J. Thomson, and J. Albert, "Optical fiber refractometer using narrowband cladding-mode resonance shifts," Appl. Opt. **46**(7), 1142–1149 (2007).
28. J. Albert, L. Shao, and C. Caucheteur, "Tilted fiber Bragg grating sensors," Laser Photonics Rev. **7**(1), 83–108 (2013).
29. T. Guo, Á. González-Vila, M. Loyez, and C. Caucheteur, "Plasmonic optical fiber-grating immunosensing: a review," Sensors **17**(12), 2732 (2017).
30. Y. Schevchenko, T. J. Francis, D. A. D. Blair, R. Walsh, M. C. DeRosa, and J. Albert, "In situ biosensing with a surface plasmon resonance fiber grating aptasensor," Anal. Chem. **83**(18), 7027–7034 (2011).
31. X. Chen, Y. Nan, X. Ma, H. Liu, W. Liu, L. Shi, and T. Guo, "In-Situ detection of small biomolecule interactions using a plasmonic tilted fiber grating sensor," J. Lightwave Technol. **37**(11), 2792–2799 (2019).
32. F. Chiavaioli, F. Baldini, S. Tombelli, C. Trono, and A. Giannetti, "Biosensing with optical fiber gratings," Nanophotonics **6**(4), 663–679 (2017).
33. V. Márquez-Cruz and J. Albert, "High resolution NIR TFBG-assisted biochemical sensors," J. Lightwave Technol. **33**(16), 3363–3373 (2015).
34. G. Laffont and P. Ferdinand, "Tilted short-period fibre-Bragg-grating- induced coupling to cladding modes for accurate refractometry," Meas. Sci. Technol. **12**(7), 765–770 (2001).
35. M. E. Bosch, A. J. R. Sánchez, F. S. Rojas, and C. B. Ojeda, "Recent development in optical fiber biosensors," Sensors **7**(6), 797–859 (2007).
36. M. Sypabekova, S. Korganbayev, Á. González-Vila, C. Caucheteur, M. Shaimerdenova, T. Ayupova, A. Bekmurzayeva, L. Vangelista, and D. Tosi, "Functionalized etched tilted fiber Bragg grating aptasensor for label-free protein detection," Biosens. Bioelectron. **146**, 111765 (2019).
37. I. Pethes, "The structure of aqueous lithium chloride solutions at high concentrations as revealed by a comparison of classical interatomic potential models," J. Mol. Liq. **264**, 179–197 (2018).
38. C. Caucheteur, M. Loyez, Á. González-Vila, and R. Wattiez, "Evaluation of gold layer configuration for plasmonic fiber grating biosensors," Opt. Express **26**(18), 24154–24163 (2018).
39. Y. Y. Shevchenko and J. Albert, "Plasmon resonances in gold-coated tilted fiber Bragg gratings," Opt. Lett. **32**(3), 211–213 (2007).
40. E. M. Hassan, W. G. Willmore, B. C. Mckay, and M. C. Derosa, "In vitro selections of mammaglobin A and mammaglobin B aptamers for the recognition of circulating breast tumor cells," Sci. Rep. **7**(1), 14487 (2017).
41. M. Gijs, G. Penner, G. B. Blackler, N. R. E. N. Impens, S. Baatout, A. Luxen, and A. M. Aerts, "Improved aptamers for the diagnosis and potential treatment of HER2-positive cancer," Pharmaceuticals **9**(2), 29 (2016).